Colloid Polym Sci (2002) 280: 798–813
DOI 10.1007/s00396-002-0683-2

ORIGINAL CONTRIBUTION

N. Grozev
V. Aguié-Béghin
T. Ivanova
S. Baumberger
B. Cathala
R. Douillard
I. Panaiotov

State, electrical and rheological properties of model and dioxan isolated lignin films at the air–water interface

Received: 27 August 2001
Accepted: 15 March 2002
Published online: 22 May 2002

N. Grozev (✉) · T. Ivanova · I. Panaiotov
Biophysical Chemistry Laboratory,
University of Sofia, J. Bourchier str. 1,
1126 Sofia, Bulgaria
E-mail: fhng@chem.uni-sofia.bg

V. Aguié-Béghin · B. Cathala
R. Douillard
Unité Mixte de Recherche Fractionnement des Agro-Ressources et Emballage, INRA, CRA, 2 Espl. R. Garros, BP224,
51686 Reims Cedex 2, France

S. Baumberger
Laboratoire de Chimie Biologique, Institut National Agronomique Paris-Grignon,
78850 Thiverval Grignon, France

Abstract The properties of monolayers of the dioxan lignin and of model dehydrogenation polymers spread at the air–water interface were investigated by the following techniques: surface pressure, surface potential, ellipticity, rheological analysis and molecular modeling. Information about the state of the monolayer was obtained from surface pressure–area and surface potential–area isotherms. At small deposited quantities (1–2 mgm^{-2}) a quasi-monolayer (2D) structure is formed. The values obtained for the mean area per monomer and for the mean dipole moment are coherent with previously reported data, as well as with the proposed molecular model. At higher deposited quantities (3–6 mgm^{-2}) a complex 3D network is built. These statements are supported by the results obtained by means of ellipsometry and surface rheology. Ellipsometry provides data for the stability of the 2D structure and for the slightly unstable 3D network. By using an original rheological approach, both structures are distinguished by their mechanical response when a dilatational stress is applied. The quasi-monolayer structure behaves as an elastic 2D medium during the compression, while two relaxation processes with characteristic times of 10 and 100 s were observed. The 3D network behaves as a Maxwell viscoelastic body during the compression, while three relaxation processes with characteristic times of 1, 10 and 100 s were detected.

Keywords Monolayers · Lignin · Dehydrogenation polymers · Ellipsometry · Surface rheology

Introduction

Lignin is a very complex macromolecule constituted by phenylpropane monomers linked through 11 different types of covalent bonds [1, 2, 3] and forming a 3D network determining many specific properties of the plant cell walls. It is the second-most abundant natural polymer and an attractive object for investigations.

The considerable interest in this polymer can be divided into a fundamental and a practical part. The former concerns the cytological structure and the role of lignin in the plant cell walls as well as the interactions with other polymers, such as polysaccharides. It is assumed that this polymer is responsible to some extent for the mechanical properties of the plant cell wall and that it may also control the water permeability and antibacterial resistance. The second interest is related to the necessity to find more and proper applications of the lignins, eliminated as waste products of the paper industry. The biodegradation of lignin is a link between these distinct parts.

It is worth mentioning that in the listed areas the processes occurring at the interfaces are of great importance. A few reasons can be cited. The plant cell wall

is a heterogeneous system constituted of cellulose, lignin and hemicelluloses. The interactions between them should depend on the interface of the contact zone. Some lignins are used to stabilize different emulsions; this involves a process of adsorption at the interface [4]. A general common feature of the degradation processes is that they take place most often at the interfaces rather than in the bulk of a solution. Here the efficiency of the reactions depends on the physical state and on the accessibility of the substrate.

As we assume the importance of the interfacial phenomenon in lignin chemistry, a simplified but realistic system mimicking the interfacial structure of the polymers studied, such as lignin films at the air–water interface, can be used. The monomers which constitute lignins possess the necessary properties for forming interfacial films – polar groups (hydroxyl, phenolic, etc.) and an apolar carbon backbone. The monolayer approach is characterized by the ability to control and modify the interfacial organization of the substrate by varying the surface pressure.

During the past 30 years there have been several reports [4, 5, 6, 7, 8, 9, 10, 11, 12] dedicated to the study of the properties of lignin monolayers at the air–water interface with different methods (surface pressure–area and surface potential–area isotherms, ellipsometry, Langmuir–Blodgett films, neutron reflectivity).

The basic facts gathered by those investigations can be summarized as follows:

1. There is a great dependence of the properties on the origin and the method of preparation of the lignin samples [5].
2. From the surface pressure–area, $\pi(A)$, isotherms the apparent area per monomer at close packing was obtained to be 10–17 $Å^2$ for all the lignins studied [4, 6]. The thickness of the films increases with the amount deposited. Its value was established to be between 15–96 Å [7] and 60 Å for Langmuir–Blodgett films made of lignins [8].
3. The role of the compression rate on the isotherms was considered [6, 9]. A particular rheological behavior was observed and an attempt to model it was made [10].
4. The stability of the monolayer increases with the molecular size owing to the large number of potential hydrogen-bonding sites [4].
5. The influence of pH was checked and it was shown that at acidic pH values aggregation between molecules occurs [11].
6. It was suggested that the use of dehydrogenation polymers (DHPs) is a fruitful approach for obtaining information concerning the structure and properties of natural lignins. Indeed DHPs can be synthesized in a reproducible way and free from contamination by carbohydrates which can alter the surface behavior of lignins. DHPs can be of guaiacyl (DHPG) and guaiacyl/syringyl (DHPGS) type. By neutron reflectivity [12] it was demonstrated that both DHPs form a nohomogeneous structure with the DHP distribution going from a dense structure at the air side to a dilute one at the water side.

The aim of the present work is to study the state, electrical and rheological properties of model DHP films and natural grass lignin. The roles of the mode of formation of the lignin films and of the pH on the state and rheological properties were investigated.

Materials and methods

Materials

Detailed information about the synthesis and characterization of the model polymers (DHPs) used in this work can be obtained from Ref. [12]. Organosolv lignin (D-L) was dioxan-extracted from wheat straw. It is worth mentioning that there are 3 wt% sugars and 3.5 wt% esterified phenolic acids in this lignin. The preparation and characteristics of the sample are described in Ref. [10].

Dioxan used as solvent was supplied by Fluka. HCl and NaOH were purchased from Merck. Na_2HPO_4 was a product of Theokom (Sofia, Bulgaria). In all the experiments, doubly distilled water was used.

Measurements at the air–water interface

The polymers under study were dissolved in a dioxan and water mixture (9:1) at a concentration of 2 gl^{-1}.

The formation of polymer monolayers was performed by droplet deposition of a specified amount of the solutions (calculated in milligrams per square meter) over the available area of a Teflon trough (440 cm^2).

The surface pressure, π, was measured using a KSV-2200 (Finland) surface balance equipped with a platinum plate. The surface potential, ΔV, was measured simultaneously by using a gold-coated ^{241}Am ionizing electrode, a reference electrode and a KP 511 (Kriona, Bulgaria) electrometer, connected to a personal computer provided with user software for real-time data measurements. As usual, the surface potential of the pure aqueous surface fluctuated for about 30 min. When the air–water surface potential became constant, spreading of the monolayer could be performed. The accuracy of the initial surface potential value was ± 15mV.

Five kinds of experiments were performed and all the experiments were performed at 20 ± 2 °C.

Surface pressure–area and surface potential–area isotherms

Surface pressure–area and surface potential–area isotherms were obtained after spreading the solution on the aqueous subphase with three different pH values: pH 1.2 (0.1 N HCl); pH 5.8 (doubly distilled water); pH 11 (0.025 M Na_2HPO_4–NaOH buffer). The quantities spread were 1, 2, 3, 4, 5 and 6 mgm^{-2}. After the deposition of the monolayer, from the dioxan–water solution, the surface potential was allowed to reach a constant value (about 5 min). Then, the monolayer was compressed with a constant velocity, U_b, of 10 cm^2min^{-1}. At this rate, maximum reproducibility was obtained. As already mentioned there is a dependence on the velocity of compression: if the compression is performed at a slower rate, the isotherm shifts slightly to the left. Besides this, the compressions with $U_b = 10$ cm^2min^{-1} were used to avoid possible contamination

from the atmosphere during the prolonged compressions. The addition of 1% amyl alcohol in the spreading solution, commonly used for a high yield of protein spreading, did not change the isotherms dramatically. In the pioneer work of Luner et al. [4] the influence of the position of the Wilhelmy plate on the $\pi(A)$ isotherms was pointed out. The position of the platinum plate in our experiments was perpendicular to the movable barrier because it was observed [4] that when the plate is parallel to the barrier the plate is displaced to some angle of the normal at high compressions.

For the sake of a clear presentation of the results, in the Results and discussion the isotherms are shown for 1, 2, 3 and 6 mgm^{-2} only. The apparent area per monomer was calculated using mean monomer weights of 200 (for DHPGS and D-L) and 180 for DHPG. The experimental ΔV curves presented are smoothed, by appropriate treatment using the commercial program Table Curve.

The decrease of the surface area and the evolution of $\Delta V(t)$ at constant surface pressure

The decrease of the surface area, $\Delta A(t)$, and the evolution of $\Delta V(t)$ at constant surface pressure were measured for 2 and 6 mgm^{-2} spread quantities. The subphases used were aqueous solutions with different pH. A dependence on the rate of the barrier movement as well as on the value of the constant surface pressure was observed. For this reason the following procedure was adopted: spreading of a given quantity, waiting 5 min and consecutive compression with $U_b = 10$ cm^2min^{-1} until an increase of 1.5–2 mNm^{-1} in the surface pressure was reached. The barostat system was then turned on.

The evolution of the surface pressure at constant area

The evolution of the surface pressure, $\pi(t)$, at constant area, after stopping the continuous compression ($U_b = 15$ cm^2min^{-1}) of the monolayer for 2 and 6 mgm^{-2} spread quantities was measured. The subphases used were aqueous solutions with three pH.

Surface rheology experiments

Surface rheology experiments consist of measuring the surface pressure variations at several distances, x_i, as a function of time during and after a small compression ($\Delta\pi = 0.5$ mNm^{-1}) of the monolayer (Fig. 1). Two spread quantities were investigated: 2 and 6 mgm^{-2}. The compressions of the initially quasi-stable interfacial film were performed with two velocities $U_b = 180$ and 10 cm^2min^{-1} for each distance x_i. To ensure an initially quasi-stable state of the monolayers, the following procedure was used. The monolayers of 2 mgm^{-2} were built and 5 min was allowed before compression with $U_b = 10$ cm^2min^{-1} until 2.5 mNm^{-1} was performed. Then another period of 15 min was allowed. In the case of 6 mgm^{-2} the monolayer was built and a period of 20 min was allowed, without further compression.

Ellipsometry

The monolayers were investigated by means of ellipsometry. The measurements were performed using a spectroscopic phase-modulated ellipsometer (UVISEL, Jobin Yvon, Longjumeau, France). It was equipped with a xenon arc lamp. The chosen configuration was the following: the polarizer and the analyzer were set to 45°, the photoelastic modulator, activated at a frequency of 50 kHz, was set to 0° orientation.

The measurements were monitored at an angle of incidence of 53.4°. The two ellipsometric angles ψ and Δ are linked to the two reflectivity coefficients r_p and r_s in directions parallel and perpendicular to the incidence plane, respectively, by

$$\frac{r_p}{r_s} = tg\Psi \exp(i\Delta). \tag{1}$$

The fixed wavelength chosen for the kinetic measurements corresponds to the Brewster conditions of the substrate defined by

$$\Delta = \pm\frac{\pi}{2}. \tag{2}$$

The ellipticity coefficient of the absorption layer at the Brewster conditions, $\bar{\rho}_B$, is defined by

$$\bar{\rho}_B = tg\Psi \sin\Delta. \tag{3}$$

The ellipticity measured at this angle is very sensitive to any structure at the interface, and the magnitude of the ellipticity is indicative of the number of adsorbed molecules [13].

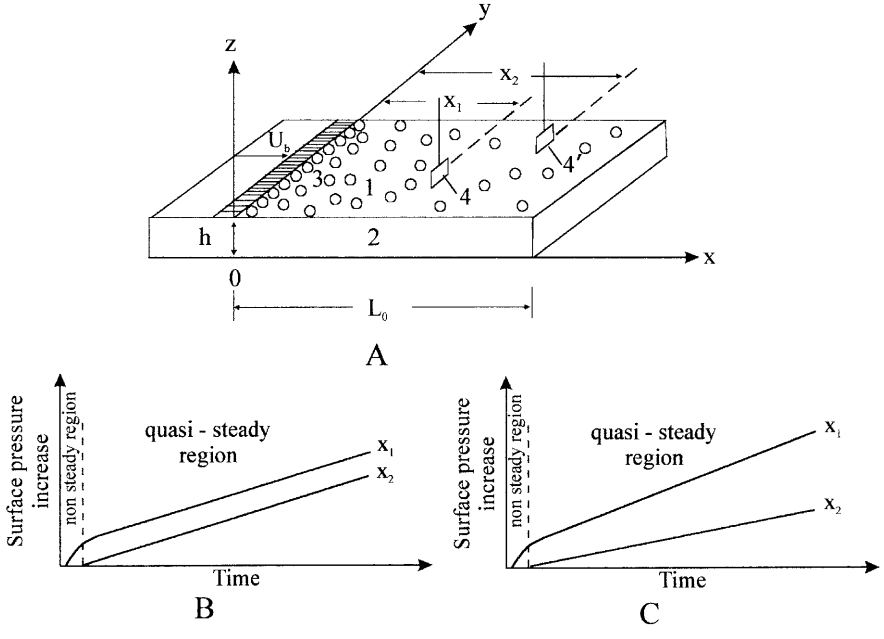

Fig. 1. **a** Method of continuous compression (or expansion): *1*: monolayer with length L_0; *2*: aqueous subphase with depth h; *3*: barrier moving with constant rate U_b; *4*, *4′*: Wilhelmy plates. **b** Variations of $\Delta\pi(x, t)$ in an elastic monolayer. **c** Variation of $\Delta\pi(x, t)$ in a viscoelastic monolayer

Molecular models

Molecular models of the lignin 10-mer at the interface were created using the commercial program HyperChem based on semiempirical quantum chemical calculations. The periodic box tool was employed to mimic the gas–water interface. It is based on a Monte Carlo distribution of water molecules in a given volume, applying also periodic boundary conditions. It is noteworthy that quantum-chemical computations cannot account for the lateral interactions originating from constant pressure application. The impossibility to introduce the lateral pressure into quantum-chemical calculations may be replaced by considering the tightest packing, corresponding to the energy minimum.

Theoretical consideration

Interpretation of surface potential data

The interpretation of ΔV data is based on the Schulman and Rideal definition of the surface potential, ΔV, for charged monolayers as the sum of the contributions of the dipole moments and of the double layer of counterions [14]:

$$\Delta V = 4\pi\mu_{\perp}\Gamma + \psi_0, \tag{4}$$

where $\mu_{\perp} \equiv \frac{\mu}{\varepsilon'}$ is the mean value of the sum of the vertical components of the dipole moments in one monomer, ϵ' is the dielectric constant in the plane of the monolayer, Γ is the surface density of the monomers, and ψ_0 is the electrostatic potential in the plane of the interface relative to the subjacent aqueous phase, containing monovalent counterions. In the absence of net charges at strong acidic pH, the value for ΔV is given by the first term in Eq. (4):

$$\Delta V_{\mathrm{ac}} = 4\pi\mu_{\perp}\Gamma. \tag{5}$$

The most frequently used expression for ψ_0 is based on the Gouy–Chapman classical theory of the diffuse double layer:

$$\psi_0 = \frac{2kT}{e_0}\sinh^{-1}\left(\frac{e_0 s^-}{(2n_i\varepsilon kT/\pi)^{1/2}}\right), \tag{6}$$

where s^- is the number of charges per square centimeter, $\sigma = e_0 s^-$ is the charge per square centimeter of a plane, impenetrable, uniformly charged surface, n_i is the concentration of the monovalent counterions in the bulk, presented as point charges, being able to approach the charged plane, ϵ is the dielectric constant of water, k is the Boltzmann constant, T is the absolute temperature, and e_0 is the electrostatic charge.

Let us consider, as a first approximation, that the appearance of negatively charged monomers (due to the dissociation of the phenyl groups at alkaline pH) does not modify the dipole moment $\mu_{\perp}$ of the monomer and the monomer density, Γ. Then, by using Eqs. (5) and (6), Eq. (4) becomes

$$\Delta V_{\mathrm{alk}} = \Delta V_{\mathrm{ac}} - \frac{2kT}{e_0}\sinh^{-1}\left(\frac{e_0 s^-}{(2n_+\varepsilon kT/\pi)^{1/2}}\right). \tag{7}$$

From Eq. (7), the corresponding Graham equation can be used to estimate the number of charges per square centimeter:

$$s^-(t) = \frac{1}{e_0}\sqrt{\frac{2n_+\varepsilon kT}{\pi}}\sinh\frac{e_0(\Delta V_{\mathrm{ac}} - \Delta V_{\mathrm{alk}})}{2kT}. \tag{8}$$

Rheological dilatational properties

The dynamic response of a surface film to a dilatational (compressional) mechanical stress has been investigated over a long time scale: $10^{-6} < t < 10^3$ s. Data for the viscoelastic dilatational properties of surface films have been obtained in several ways:

1. Analysis of thermally excited surface waves, probed by surface light scattering. This is for characteristic times in the range 10^{-6}–10^{-3} s [15, 16, 17].
2. Mechanically generated surface waves by periodic compression–expansion of the surface film. This is for characteristic times in the range 10^{-3}–1 s [18, 19, 20, 21, 22].
3. Continuous compression (or expansion) of a surface for characteristic times in the range 1–10^3 s [23, 24, 25, 26, 27, 28, 29, 30, 31].

In general, the viscoelastic properties of a surface film depend on the characteristic time of the perturbation, since various relaxation processes involving various molecular relaxation mechanisms with different characteristic times can take place.

The method of continuous compression of a surface film [24, 25, 26] consists of compressing the monolayer by means of a barrier moving with a constant velocity U_{b} (Fig. 1a). As a result of the surface density gradient, caused by the continuous local surface pressure perturbation, the simultaneous motion of the monolayer and of the liquid substrate occurs (so-called Marangoni effect). The surface motion is practically dilatational and can be detected by measuring the change of any surface parameter [24, 25, 26]. As it is shown in Fig. 1, the changes in the local surface pressure were measured at points x_1 and x_2 using two Wilhelmy plates 4 and 4′.

In order to describe the simultaneous longitudinal motion of the surface film and of the liquid subphase, the

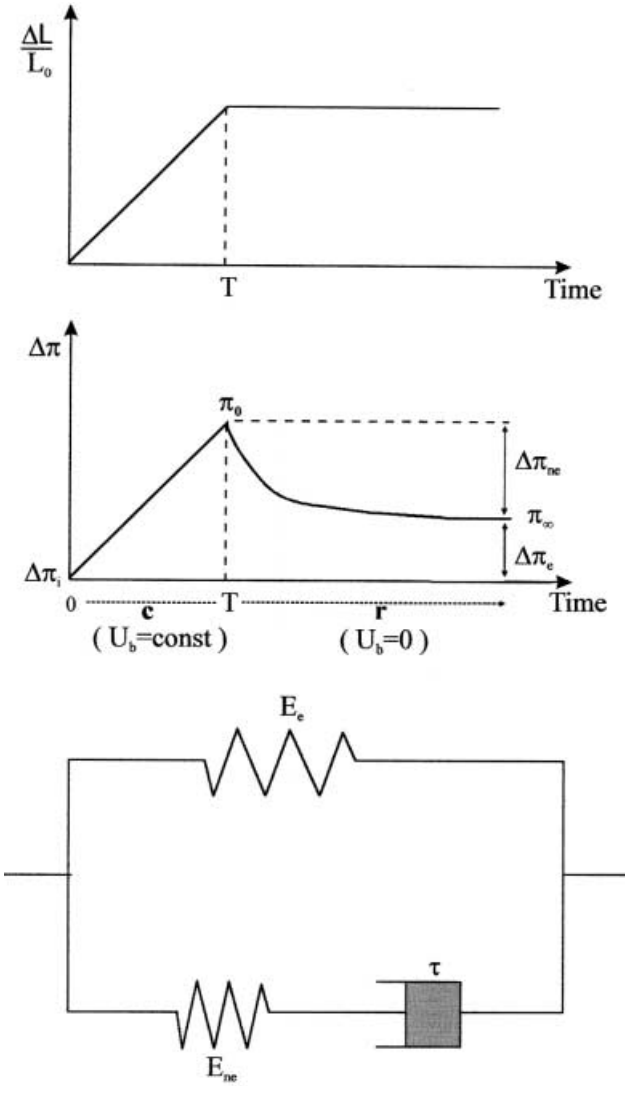

Fig. 2. Rheological model of the monolayer. Deformation $\Delta L/L_0$ and change of surface pressure, $\Delta\pi$, during the time, T, of compression, c, with constant velocity U_b ($\Delta L \equiv U_b t$), followed by a relaxation, r

following assumptions corresponding to the experimental conditions were made [23, 24, 25, 26, 27, 28, 29, 30]:

1. The disturbances of the surface concentration, $\Delta\Gamma$, and of the surface pressure, $\Delta\pi$, are small compared to the initial equilibrium values of the surface concentration, Γ_0, and the surface pressure, π_0.
2. The motion in the viscous aqueous subphase is given by the Navier–Stockes equation simplified for a thin layer.

In the absence of intrinsic surface dilatational viscosity or other relaxation processes, the rheological behavior of an insoluble monolayer is elastic. In this simplest case, the following differential equation governs

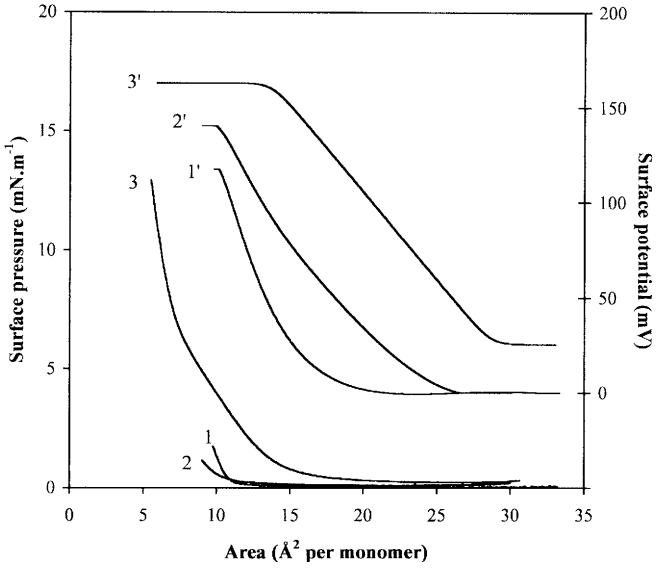

Fig. 3. Surface pressure–apparent area per monomer, $\pi(A)$, and corresponding surface potential–apparent area, $\Delta V(A)$, ($'$) isotherms for spread quantity of 1 mgm^{-2} on a subphase with pH 5.8. Curves *1* and *1′*: dioxan lignin (*D-L*); curves *2* and *2′*: dehydrogenation polymers of guaiacyl type (*DHPG*); curves *3* and *3′*: dehydrogenation polymers of guaiacyl/syringyl type (*DHPGS*). The saturation of the ΔV potential indicates a closely packed monolayer

Table 1. Apparent area per monomer at close molecular packing, A_A, corresponding a surface potential, ΔV_{sat}, a mean value of the sum of the vertical components of the dipole moment, $\mu_\perp$, and number of charges per square centimeter, s^-, for monolayers of lignins (dioxan lignin, *D-L*, dehydrogenation polymers of guaiacyl type, *DHPG*, dehydrogenation polymers of guaiacyl/syringyl type, *DHPGS*)., spread on a subphase with various pH

pH	Polymer	A_A (Å^2)	ΔV_{sat} (mV)	$\mu_\perp$ (mD)	s^- (10^{-13})
1.2	D-L	14	202	75	0
	DHPG	11	247	81	0
	DHPGS	14	294	109	0
5.8	D-L	10	117	75	–
	DHPG	10	140	81	–
	DHPGS	13	162	109	–
11.2	D-L	15	108	75	2.19
	DHPG	12	164	81	1.74
	DHPGS	15	212	109	1.7

the propagation of the momentum motion along the monolayer and describes the distribution of the surface velocity, $u(x, t)$, along the coordinate x with time t:

$$\frac{\partial u}{\partial t} = D_u \frac{\partial^2 u}{\partial x^2}, \tag{9}$$

where $D_u = E_d h/4\mu$, E_d is the surface dilatational elasticity of the monolayer, μ is the bulk viscosity and h is the depth of the liquid subphase.

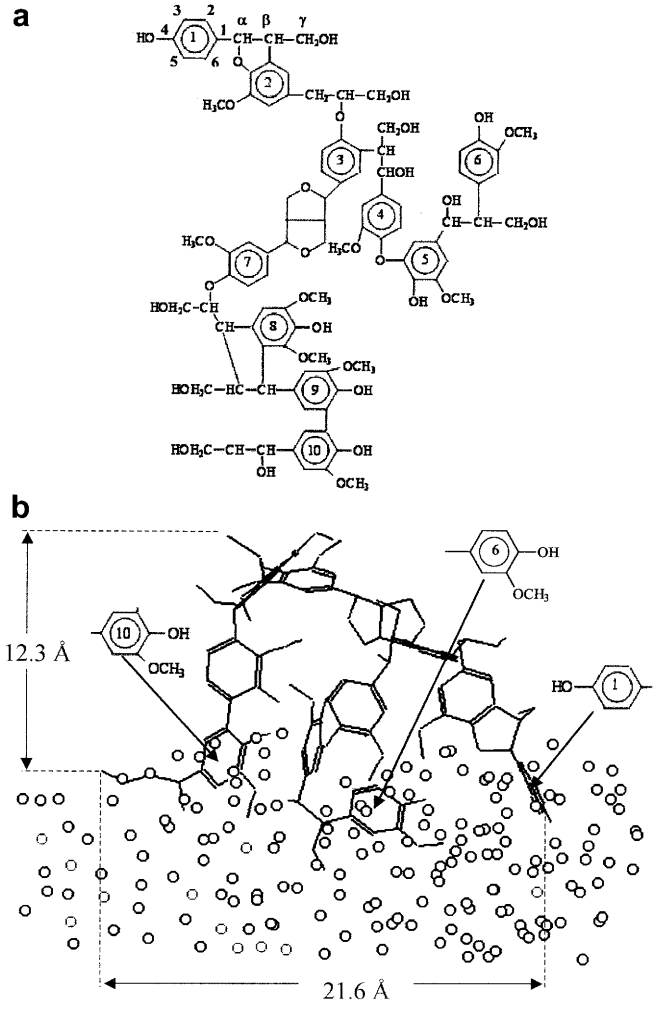

Fig. 4. **a** Structural formula of a part of a typical structure of a lignin molecule from Ref. [35], to visualize schematically a 10-mer. The carbon atom numbering of a lignin monomer is shown in the *upper left corner*. The aromatic ring is numbered 1–6 and the propane side chain α–γ [1, 2]. **b** Molecular model representing the lignin10-mer as an element of a 2D organized film. The molecular dimensions of this fragment are length 21.6 Å, width 12 Å, height 12.3 Å. The simulated air–water interface is represented by 90 water molecules (*open circles*) in contact with the lignin 10-mer

The quantity D_u may be called a surface pseudodiffusion coefficient of the surface local momentum along the interface. The quantity $\sqrt{D_u}$ represents the characteristic length of the surface velocity propagation over 1 s and depends on the rheological parameters of the surface (E_d) and of the bulk phase (μ). The characteristic

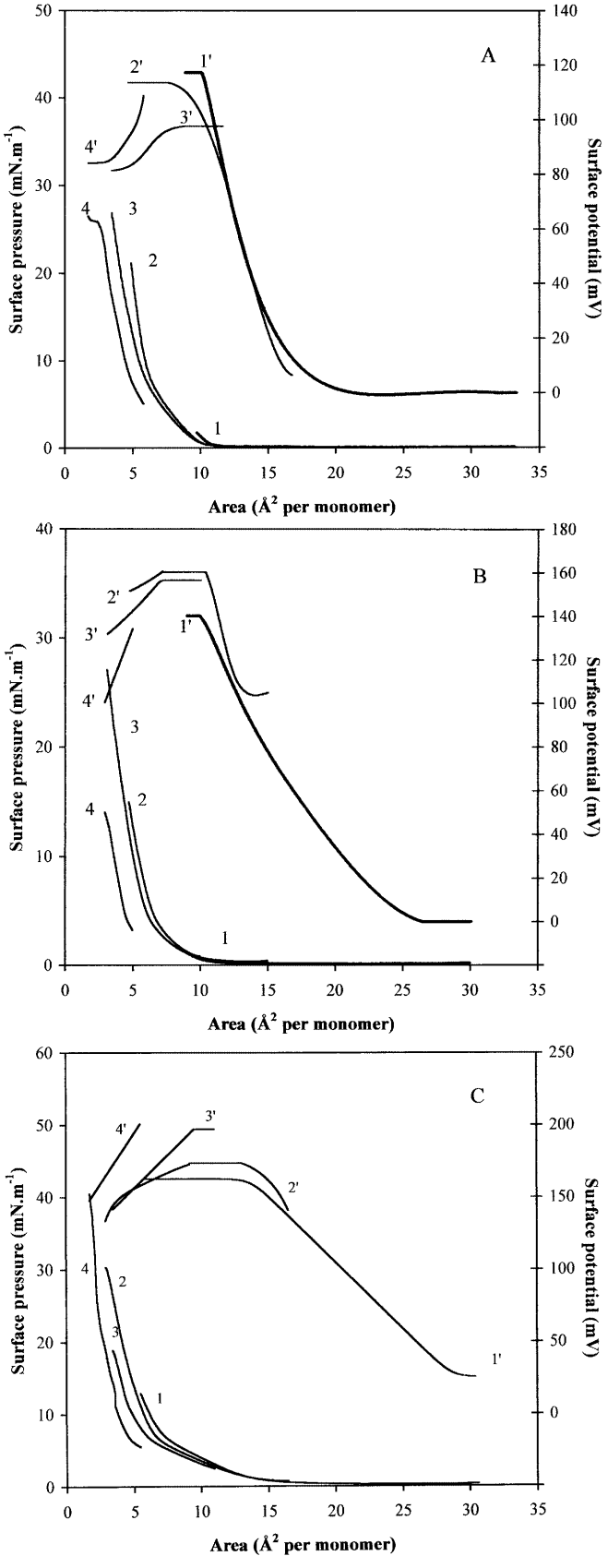

Fig. 5a–c. $\pi(A)$ and corresponding $\Delta V(A)$ ($'$) isotherms for different spread quantity of lignins on a subphase with pH 5.8. **a** D-L, **b** DHPG, **c** DHPGS. Curves *1* and *1′*: 1 mgm^{-2}; curves *2* and *2′*: 2 mgm^{-2}; curves *3* and *3′*: 3 mgm^{-2}; curves *4* and *4′*: 6 mgm^{-2}

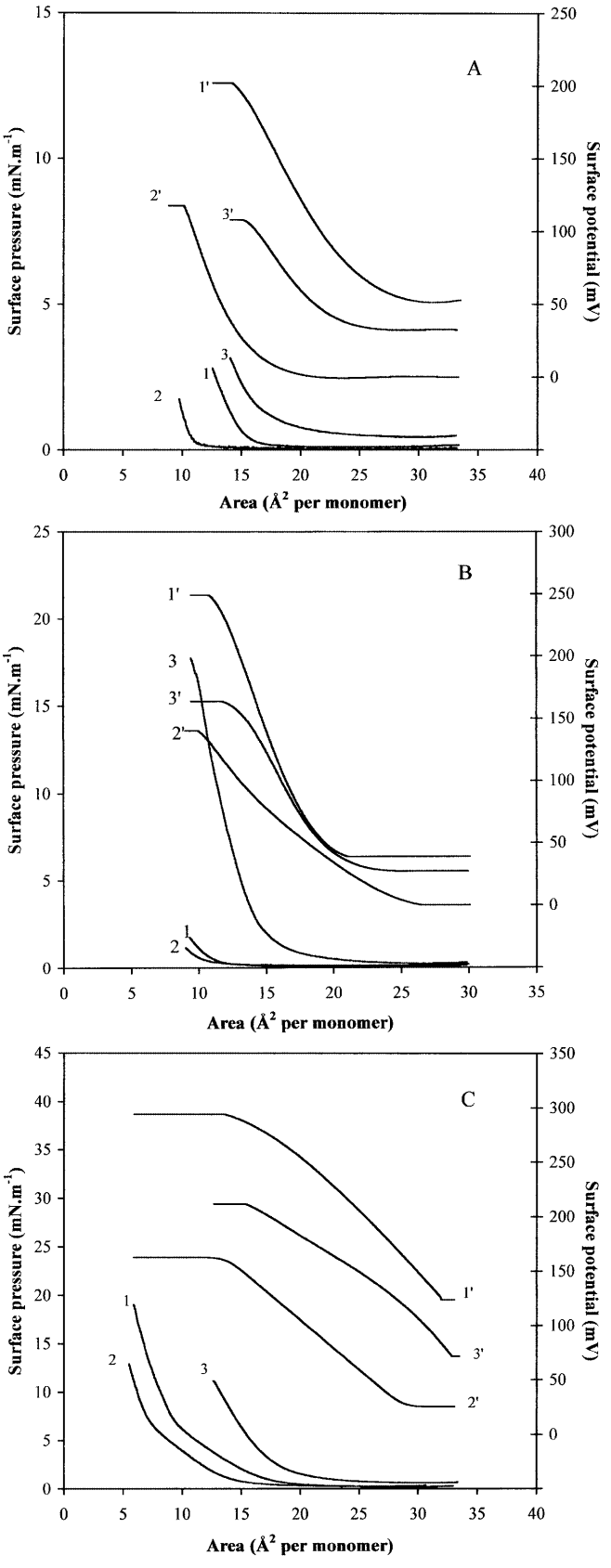

Fig. 6a–c. The influence of the pH of the subphase on the $\pi(A)$ and $\Delta V(A)$ (′) of 1 mgm^{-2} spread quantity of lignins. **a** D-L, **b** DHPG, **c** DHPGS. curves *1* and *1′*: pH 1; curves *2* and *2′*: pH 5.8; curves *3* and *3′*: pH 11.2

time of propagation along the length L_0 of an elastic monolayer is

$$\tau_M = \frac{L_0^2}{D_u}. \tag{10}$$

This characteristic time marks the transition between a nonsteady region from the beginning of the compression to $\frac{L_0^2}{D_u}$ and a quasi-steady region from $\frac{L_0^2}{D_u}$ to the end of the compression.

For the quasi-steady region of the compression established after the "arrival" of the surface pressure perturbation at the end of the trough [24, 25, 26]

$$\left(\frac{\partial u}{\partial t} = 0 \text{ while } \frac{\partial \Gamma}{\partial t} \neq 0; \frac{\partial \pi}{\partial t} \neq 0\right)$$
$$\Delta\pi(x,t) = \frac{E_d U_b}{L_0} t - \frac{4\mu U_b}{h}\left(x - \frac{x^2}{2L_0} - \frac{L_0}{3}\right). \tag{11}$$

The first term in Eq. (11) is due to the rheological properties of an elastic insoluble monolayer obeying Hooke's law. Indeed, $U_b t = \Delta L$ and $\Delta\pi = E_d \Delta L / L_0$. The second one is related to the rheological properties of a Newtonian liquid with bulk viscosity μ. The physical meaning of Eq. (11) is simple. The propagation of a local surface

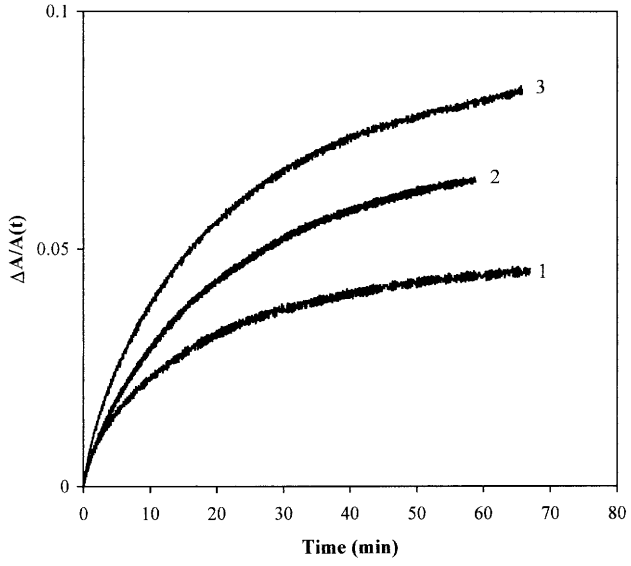

Fig. 7. Dependence of the magnitude of compression on the relative decrease of the surface area for monolayers of 3 mgm^{-2} D-L at pH 1. Curve *1*: from $\pi_{initial} = 2$ mNm^{-1} to $\pi_{constant} = 2.5$ mNm^{-1}; curve *2*: from $\pi_{initial} = 2$ mNm^{-1} to $\pi_{constant} = 3.5$ mNm^{-1}; curve *3*: from $\pi_{initial} = 2$ mNm^{-1} to $\pi_{constant} = 5$ mNm^{-1}

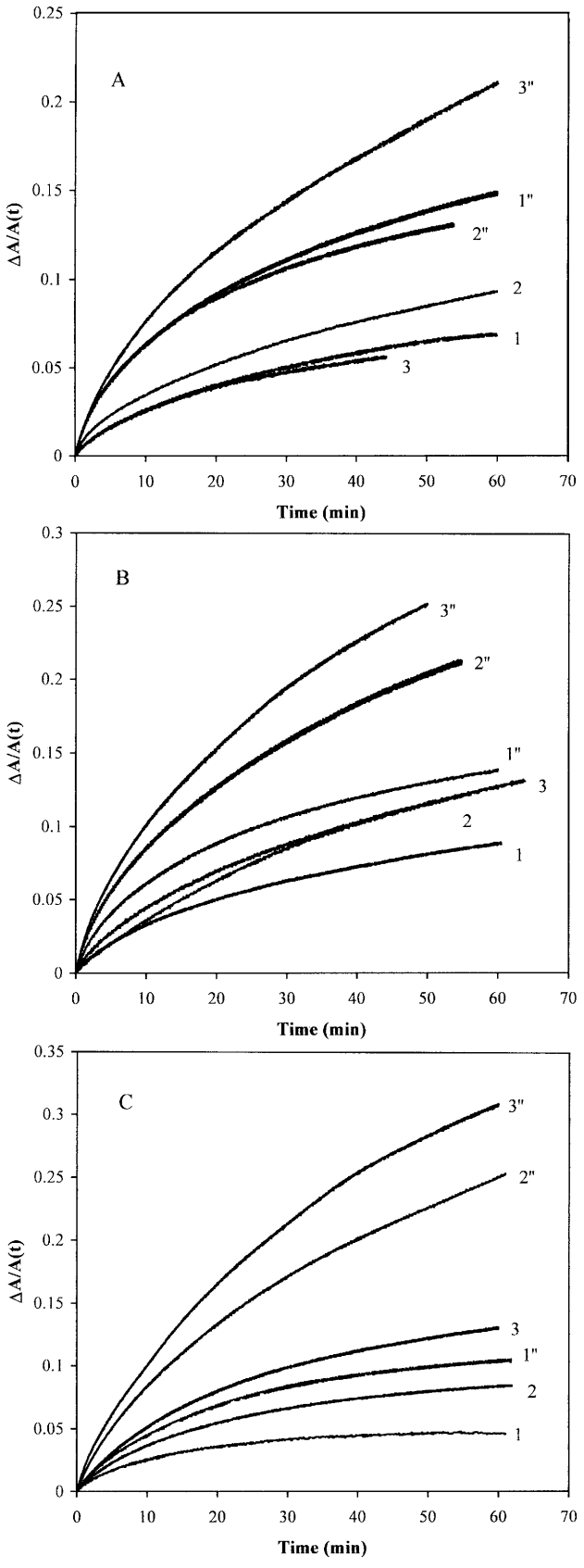

Fig. 8a–c. Relative decrease of the surface area for monolayers of 2 and 6 mgm^{-2} ($''$) spread quantity. **a** Subphase with pH 1.2, **b** subphase with pH 5.8. **c** subphase with pH 11.2. Curves *1* and *1″*: D-L; Curves *2* and *2″*: DHPG; Curves *3* and *3″*: DHPGS

density perturbation along a hypothetical free 2D elastic body must be effectuated with the velocity of sound in this 2D medium, i.e. practically instantaneously in comparison with the characteristic time of the experiment. Nevertheless, on account of the friction with the liquid subphase the propagation with the characteristic time τ_M is not instantaneous. A typical result for $\Delta\pi(x, t)$ in an elastic monolayer is presented in Fig. 1b. According to Eq. (11) the slopes $d\Delta\pi/dt$ in the quasi-steady region do not depend on the distance x.

In the case of a viscoelastic insoluble monolayer, other dissipation processes may occur in the monolayer in addition to viscous dissipation in the bulk subphase.

In order to describe the surface pressure change, $\Delta\pi = \pi(t) - \pi_i$ (Fig. 2), during the time T of the compression with a constant velocity, U_b, followed by a relaxation at constant area, we suppose that at any moment the total surface pressure change $\Delta\pi = \pi(t) - \pi_i$ can be represented as the sum of one equilibrium, $\Delta\pi_e$, and one nonequilibrium, $\Delta\pi_{ne}$, contribution:

$$\Delta\pi = \Delta\pi_e + \Delta\pi_{ne}. \tag{12}$$

The equilibrium part $\Delta\pi_e$ is related to the equilibrium surface dilatational elasticity E_e:

$$\Delta\pi_e = E_e \frac{U_b t}{L_0}, \tag{13}$$

where L_0 is the initial surface length before the compression and $\frac{U_b t}{L_0} \equiv \frac{\Delta L}{L_0}$ the corresponding strain, ϵ (Fig. 2). This elastic behavior is represented by the upper branch of the mechanical model in Fig. 2.

The nonequilibrium part of the total surface pressure change $\Delta\pi_{ne}$ is associated with the accumulation of elastic energy during the compression. Dissipation of this accumulated energy through a specific molecular mechanism occurs during compression as well as relaxation. This viscoelastic behavior can be described with Maxwell's equation:

$$\frac{d\Delta\pi_{ne}}{dt} + \frac{\Delta\pi_{ne}}{\tau} = E_{ne} \frac{\partial U}{\partial x}, \tag{14}$$

where $\Delta\pi_{ne}$ is the applied stress, E_{ne} is the nonequilibrium surface dilatational elasticity and τ is the specific time of relaxation. This viscoelastic behavior is represented by the lower branch of the mechanical model in Fig. 2. The two branches of the mechanical model are coupled in parallel according to Eq. (12), which corresponds to the addition of stresses.

Table 2. Initial and final reorganization rates and relative surface area decrease for monolayers of lignins, spread on a subphase with various pH

Quantity (mgm^{-2})	pH	Polymer	Reorganization rate (min^{-1}) at		Relative decrease of area at $t = 60$ min
			$t = 0$ min	$t = 60$ min	
[2]	1.2	D-L	0.0053	0.0006	0.069
		DHPG	0.0089	0.0008	0.095
		DHPGS	0.005	0.0002	0.057
	5.8	D-L	0.0063	0.0007	0.089
		DHPG	0.0095	0.0012	0.12
		DHPGS	0.0054	0.0006	0.13
	11.2	D-L	0.006	0.0002	0.046
		DHPG	0.0064	0.0004	0.085
		DHPGS	0.008	0.0006	0.13
[6]	1.2	D-L	0.0151	0.0008	0.15
		DHPG	0.0136	0.0007	0.13
		DHPGS	0.0145	0.0017	0.21
	5.8	D-L	0.0133	0.0012	0.14
		DHPG	0.0185	0.0013	0.21
		DHPGS	0.0203	0.0019	0.25
	11.2	D-L	0.0081	0.0002	0.11
		DHPG	0.0137	0.0027	0.25
		DHPGS	0.0188	0.0024	0.31

It would be appropriate to analyze separately the cases of relaxation processes with characteristic time τ many orders of magnitude larger than τ_M and that of relaxation processes with characteristic time θ of the order of magnitude of τ_M defined in Eq. (10).

In the first case, when $\tau \gg \tau_M$, the re-equilibration of the surface pressure gradients along x is very rapid in comparison with the surface relaxation process and we can consider the dynamic response of the monolayer as a whole, neglecting the surface pressure distribution along x. The analysis of this case based on the rheological model in Fig. 2 and Eqs. (13) and (14) gives the following equations describing the viscoelastic behavior of the monolayer [32] and the relative relaxation when the time of compression, T, is much smaller than the time of the relaxation process ($T \ll \tau$):

$$\Delta\pi = E_e \frac{U_b t}{L_0} + E_{ne} \frac{U_b \tau}{L_0} \left(1 - e^{-t/\tau}\right), \tag{15}$$

$$\frac{\Delta\pi(t) - \Delta\pi_\infty}{\Delta\pi_0 - \Delta\pi_\infty} \equiv \frac{\pi(t) - \pi_\infty}{\pi_0 - \pi_\infty} = e^{-t/\tau}. \tag{16}$$

If two slow relaxation processes with characteristic times τ_1 and τ_2 occur, the viscoelastic behavior of the monolayer is described by the model in Fig. 2 with two (instead of one) Maxwell bodies (the so-called generalized Maxwell model) [33]:

$$\Delta\pi = E_e \frac{U_b t}{L_0} + E_{ne_1} \frac{U_b \tau_1}{L_0} \left(1 - e^{-t/\tau_1}\right) + E_{ne_2} \frac{U_b \tau_2}{L_0} \left(1 - e^{-t/\tau_2}\right). \tag{17}$$

After differentiation of Eq. (17) with respect to time and with the simplification $E_{ne_1} \approx E_{ne_2} \approx \frac{E_{ne}}{2}$, the following expression for the slope $\left(\frac{d\Delta\pi}{dt}\right)_x$ during the compression can be obtained:

$$\frac{d\Delta\pi}{dt} = E_e \frac{U_b}{L_0} + \frac{E_{ne} U_b}{2} \frac{\left(e^{-t/\tau_1} + e^{-t/\tau_2}\right)}{L_0}. \tag{18}$$

According to Eq. (18) the slopes $\left(\frac{d\Delta\pi}{dt}\right)_x$ in the quasi-steady region do not depend on the distance x.

Two useful approximations describing the rheological behavior during the compression can be obtained from the general Eq. (17). When the time of compression T is much smaller (or much larger) than the times of relaxation τ_1 and τ_2, the rheological response of the surface film is elastic only. In fact, for $T \ll \tau_1$, τ_2 (realized for sufficiently rapid compression) from Eq. (17) after development in series we have

$$\Delta\pi_{(t=T)} = \Delta\pi_0 = (E_e + E_{ne_1} + E_{ne_2}) \frac{U_b T}{L_0}. \tag{19}$$

For $T \gg \tau_1$, τ_2 (realized for sufficiently slow compression) the second and the third terms of Eq. (17) can be neglected:

$$\Delta\pi_{(t=T)} = \Delta\pi_0 = E_e \frac{U_b T}{L_0}. \tag{20}$$

By using Eqs. (19) and (20) and the experimental data obtained at sufficiently rapid and slow compression, we can obtain the equilibrium, E_e, and nonequilibrium, E_{ne1} and E_{ne2}, parts of the elasticity.

For $T \ll \tau_1$, τ_2, the following expression describing the relaxation process was obtained [33]:

$$\frac{\pi(t) - \pi_\infty}{\pi_0 - \pi_\infty} = \frac{E_{ne_1}}{E_{ne_1} + E_{ne_2}} e^{-t/\tau_1} + \frac{E_{ne_2}}{E_{ne_1} + E_{ne_2}} e^{-t/\tau_2}. \tag{21}$$

In the case when $\theta \approx \tau_M$, the viscous relaxation process accompanies the propagation process along x and a fanlike dependence of the slopes $\left(\frac{d\Delta\pi}{dt}\right)$ on the distance x during the compression is observed.

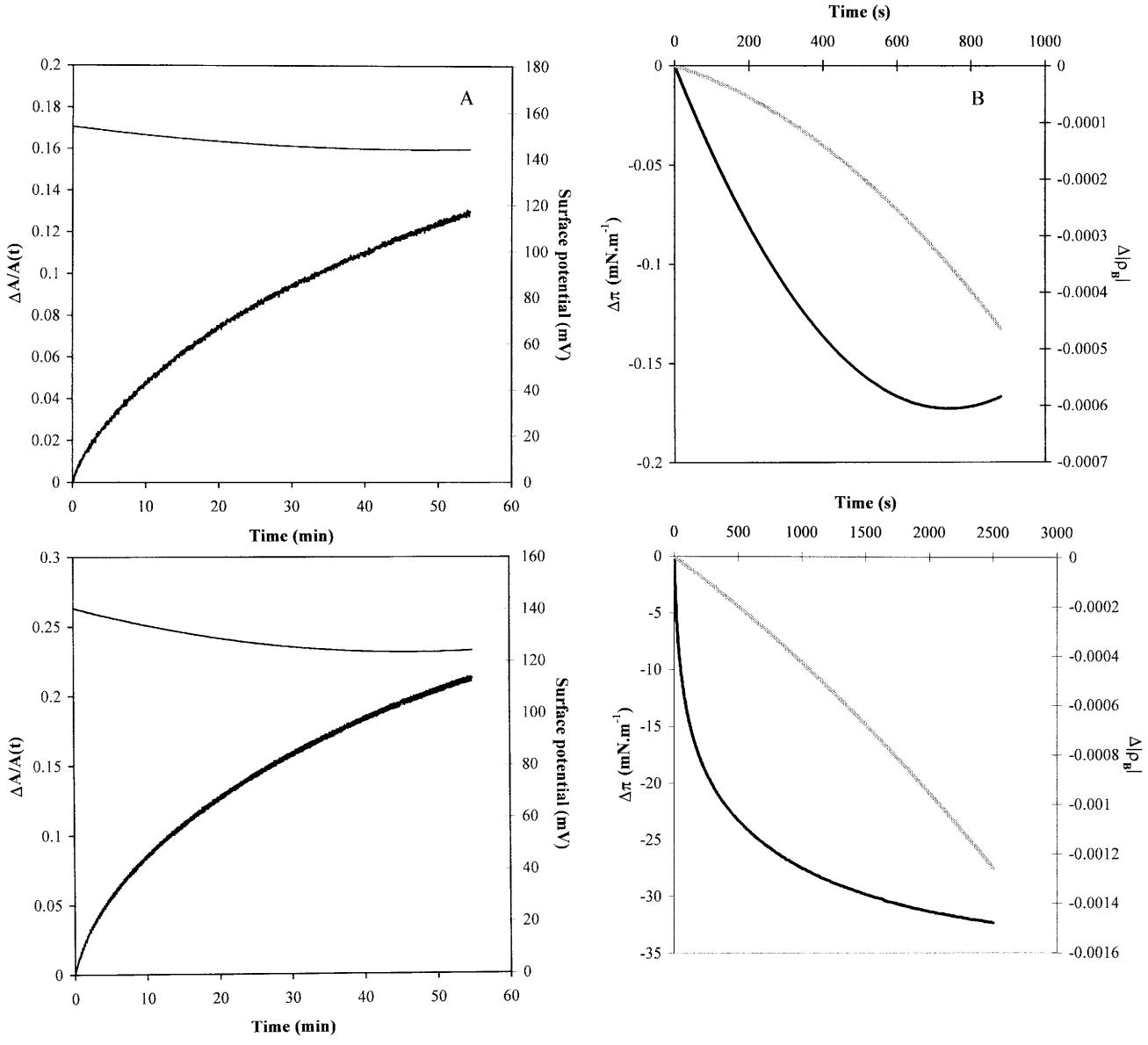

Fig. 9. **a** Relative decrease of the surface area and corresponding evolution of surface potential for monolayers of 2 (*upper*) and 6 mgm^{-2} (*lower*). **b** Evolution of the absolute value of ellipticity in Brewster-angle conditions for a spread quantity of 1 (*upper*) and 6 mgm^{-2} (*lower*) DHPG on doubly distilled water. The *thick curves* correspond to the surface pressure, while the *thin curves* correspond to the ellipticity

A typical result for $\Delta\pi(x, t)$ is presented in Fig. 1c. The nonequilibrium part of the total surface pressure change $\Delta\pi_{ne}$ is obtained by coupling the Maxwell equation (Eq. 14) with the equations describing the longitudinal momentum motion, namely the surface dynamic equation, giving the balance of forces acting on the surface and the surface mass balance equations [24, 27].

Accordingly with the model in Fig. 2 the following expression for the slope $\left(\frac{d\Delta\pi}{dt}\right)$ in the quasi-steady region of the compression is obtained:

$$\frac{d\Delta\pi}{dt} = E_e \frac{U_b}{L_0} + E_{ne} U_b \alpha \frac{\cosh \alpha(L_0 - x)}{\sinh \alpha L_0}, \tag{22}$$

where $\alpha^{-1} = \sqrt{D_u \theta}$ is the characteristic length of propagation along a viscoelastic Maxwell monolayer. For $L_0 \ll \alpha^{-1}$, i.e. for a monolayer length much smaller than the characteristic length of propagation, the viscoelastic response of the surface film to the applied stress predicted by Eq. (22) is reduced to the elastic one. Then, Eq. (22) becomes

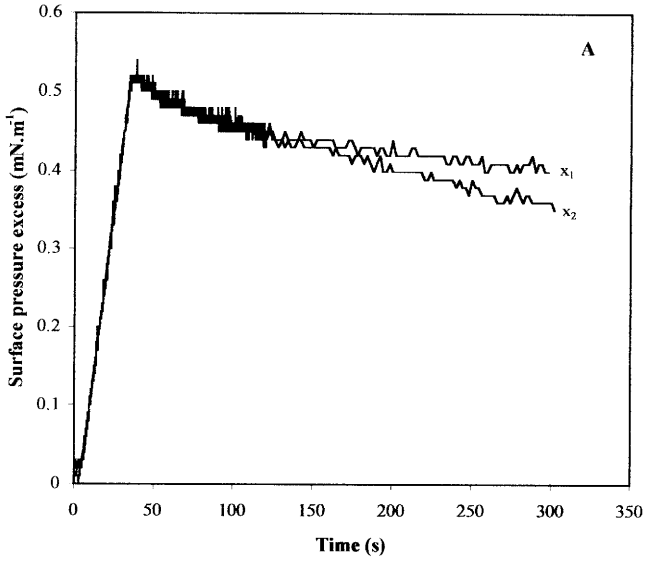

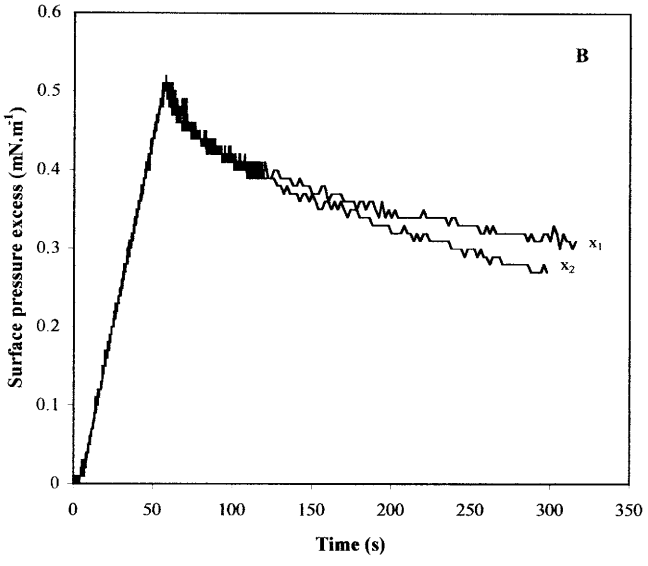

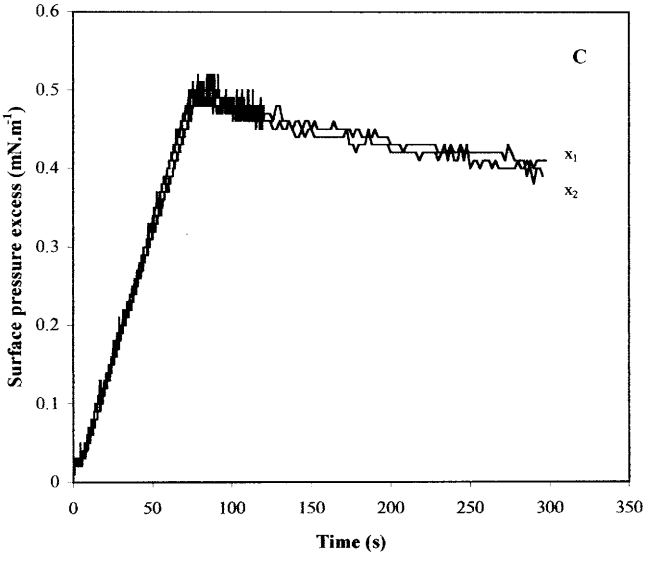

◀

Fig. 10a–c. Surface pressure change, $\Delta\pi$, with time, t, at various distances, x, during a compression with $U_b = 10$ cm^{2}min^{-1} and the consecutive relaxation of lignin monolayers with a spread amount of 2 mgm^{-2} on a subphase with pH 5.8. **a** D-L, $x_1 = 7.5$ cm, $x_2 = 18$ cm; **b** DHPG, $x_1 = 6$ cm, $x_2 = 18$ cm; **c** DHPGS, $x_1 = 4.5$ cm, $x_2 = 25$ cm

$$\frac{d\Delta\pi}{dt} = (E_e + E_{ne})\frac{U_b}{L_0}. \tag{23}$$

If two dissipation processes with different characteristic times (θ of the same order of magnitude and τ many orders of magnitude larger than τ_M) occur simultaneously, a more complex viscoelastic behavior is observed. The following expression for the slopes $\left(\frac{d\Delta\pi}{dt}\right)(x,t)$ is obtained [34]:

$$\frac{d\Delta\pi}{dt} = E_e\frac{U_b}{L_0} + E_{ne}U_b\alpha\frac{\cosh\alpha(L_0 - x)}{\sinh\alpha L_0}e^{-t/\tau}. \tag{24}$$

For $T \approx \theta$ and $T \ll \tau$ (realized for sufficiently rapid compression), the influence of the slow relaxation processes with characteristic time τ is negligible and Eq. (24) is reduced to Eq. (22).

For $T \gg \theta$, τ (realized for sufficiently slow compression), the viscoelastic response of the surface film to the applied stress is reduced to an elastic one. In fact, $\exp(-t/\tau) \to 0$ and from Eq. (24) one obtains

$$\frac{d\Delta\pi}{dt} = E_e\frac{U_b}{L_0}. \tag{25}$$

The listed equations are theoretical models that determine the rheological, dilatational properties of elastic and viscoelastic surface films. The equations are described in details in Refs. [24, 25, 26, 27, 28, 29, 30, 32, 33, 34].

Results and discussion

Effect of the spread quantity and the pH of the subphase

Typical surface pressure–apparent area per monomer, $\pi(A)$, and surface potential–apparent area per monomer, $\Delta V(A)$, isotherms obtained for 1 mgm^{-2} deposited D-L (curves 1 and 1′, respectively), DHPG (curves 2 and 2′) and DHPGS (curves 3 and 3′) on the subphase with pH 5.8 are given in Fig. 3. A quasi-monolayer organization of the polymer film can be assumed on the basis of the following observations. The ΔV potential values start from zero for dilute monolayers. Under further compression the monolayers exhibit liquid–condensed states [35] with a more pronounced expanded region for DHPGS.

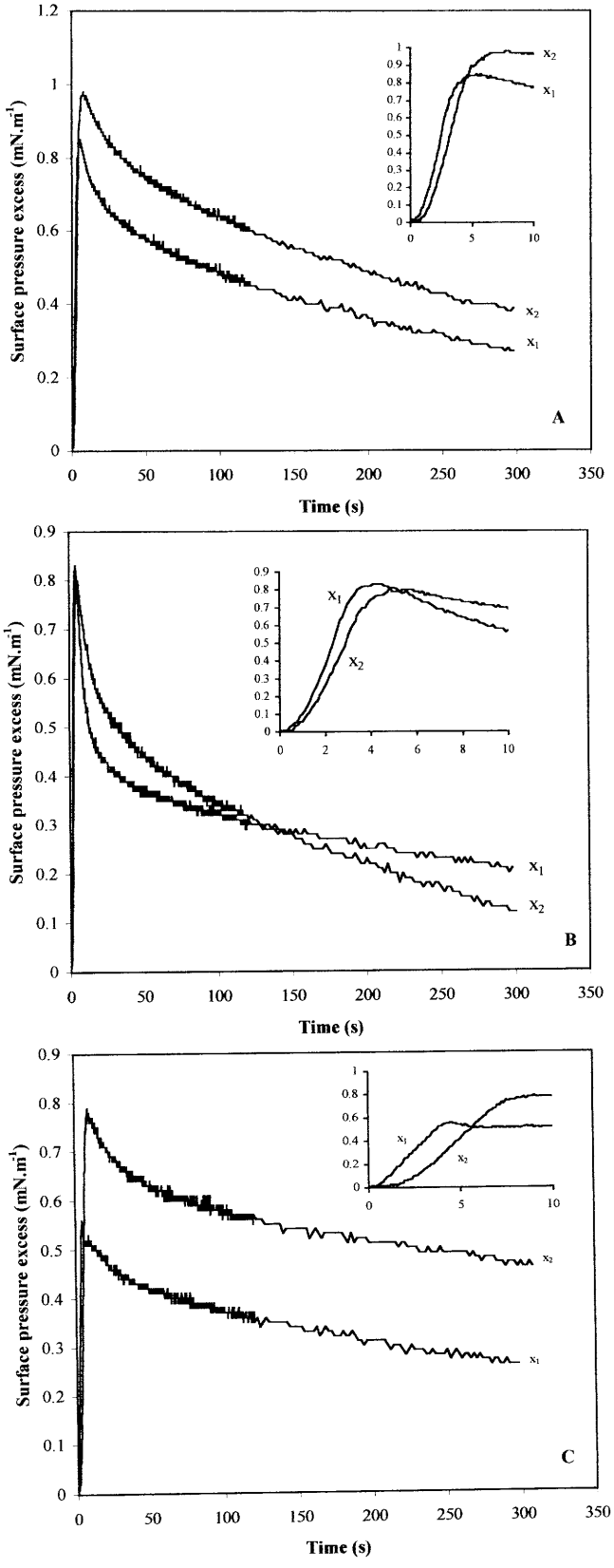

Fig. 11a–c. Surface pressure change, $\Delta\pi$, with time, t, at various distances, x, during a compression with $U_b = 180$ cm^{2}min^{-1} and the consecutive relaxation of lignin monolayers with a spread amount of 2 mgm^{-2} on a subphase with pH 5.8. **a** D-L, $x_1 = 7.5$ cm, $x_2 = 18$ cm; **b** DHPG, $x_1 = 6$ cm, $x_2 = 18$ cm; **c** DHPGS, $x_1 = 4.5$ cm, $x_2 = 25$ cm

Following the general ideas on the state of polymer films, a close packing of the 3D lignin molecules corresponds to a saturation of the $\Delta V(A)$ curves. The calculated apparent areas per monomer, the corresponding surface potential and the mean dipole moments calculated from Eq. (5) are presented together with the values obtained at pH 1.2 and 11.2 in Table 1. The values per monomer for the DHPs (10–15 Å^2) presented are of the same order of magnitude as, but slightly smaller than, those previously reported [4], probably because of the use of the dioxan–water solvent mixture. It should be mentioned that all the values obtained are smaller than the areas calculated for a molecular model assuming that the phenyl–propane monomer lies flat on the surface (about 45 Å^2). A more realistic molecular model of a ten-monomer 3D DHP molecule [36], an element of the 2D organized film, lying on a water subphase is presented in Fig. 4. The optimization supports the idea [4] that some of the monomers are in the upright position. The calculated, on the basis of the model, dimensions at closed packing are a molecular area between 15 and 26 Å^2 per monomer and a thickness of 12 Å. The slight difference between the observed (10–15 Å^2) and the model values could be due to the partial dissolution into the aqueous subphase which cannot be completely excluded and/or an aggregation process.

The more pronounced expanded region for DHPGS can be explained by the fact that a DHPGS molecule has a higher content of β-O-4 links and an increased number of methoxyl groups and could be more linear, both factors probably contributing to a higher hydrophilicity [37].

The isotherms obtained after spreading different quantities of D-L, DHPG and DHPGS are presented in Fig. 5. It is obvious that the isotherms depend on the quantity deposited. A state close to quasi-monolayer organization of the 3D lignin molecules can be considered in the case of spreading of 1–2 mgm^{-2}. When the spread surface concentration increases, the $\pi(A)$ isotherms shift to small apparent areas per monomer that differ from the corresponding values in the case where the compression starts from a more dilute initial state. For deposited quantities of 3–6 mgm^{-2} the initial values for ΔV are higher than those at close packing and start to decrease with further compression. This behavior may be due to rearrangement in a 3D layer, formed when the quantity spread is higher than needed for obtaining a monomolecular structure. In conclusion, in the case of spreading of

Table 3. Characteristic times and equilibrium and nonequilibrium elasticities for lignin monolayers spread on three different subphases

Quantity (mgm^{-2})	pH	Polymer	θ (s)	τ_1 (s)	τ_2 (s)	E_e (mNm^{-1})	E_{ne} (mNm^{-1})	$\frac{E_{ne}}{E_e+E_{ne}}100\%$
[2]	1.2	D-L	–	12 ± 1.0	135 ± 1	11 ± 1	8 ± 2	42
		DHPG	–	7.8 ± 0.9	111 ± 1	9 ± 2	17 ± 3	65
		DHPGS	–	11 ± 2.0	133 ± 15	10 ± 1	5 ± 2	33
	5.8	D-L	–	8.3 ± 0.1	139 ± 9	11 ± 3	12 ± 1	52
		DHPG	–	6.5 ± 1.3	131 ± 1	6 ± 2	17 ± 3	74
		DHPGS	–	12 ± 1.0	133 ± 3	9 ± 2	6 ± 1	40
	11.2	DHPG	–	12 ± 1	102 ± 9	9 ± 1	20 ± 1	69
[6]	1.2	D-L	0.44 ± 0.06	10.0 ± 1.0	111 ± 22	17 ± 3	39 ± 5	69
		DHPG	0.57 ± 0.14	8.3 ± 1.3	66 ± 7	13 ± 1	47 ± 8	78
		DHPGS	0.86 ± 0.04	9.0 ± 0.8	84 ± 4	8 ± 1	34 ± 2	80
	5.8	D-L	0.65 ± 0.06	9.1 ± 4	131 ± 18	13 ± 2	28 ± 4	68
		DHPG	0.63 ± 0.03	9.2 ± 1.0	89 ± 9	7 ± 1	51 ± 2	88
		DHPGS	0.61 ± 0.05	9.0 ± 1.0	113 ± 4	8 ± 1	53 ± 3	87
	11.2	DHPG	1.53 ± 0.02	12.0 ± 2	114 ± 2	6 ± 2	25 ± 3	80

3–6 mgm^{-2} the isotherms indicate the formation of a 3D network structure rather than a monolayer one.

The isotherms obtained on subphases with different pH for all the polymers studied are presented in Fig. 6. At pH 5.8 the isotherms are on the left compared to those at pH 1 and 11. The isotherms at pH 1 are shifted to higher apparent areas per monomer, probably as a consequence of additional aggregation of the molecules in a more fibrous organization [11]. At alkaline pH, the isotherms started from a higher initial surface pressure and they are more expanded as a result of the ionization and the electrostatic interactions of the phenolic groups. By using Eqs. (5) and (8) the values for $\mu_\perp$ and s^- are calculated and they are presented in Table 1. It should be stressed that generally the values for the ΔV potential as well as that for the mean vertical dipole moment are coherent with previously reported ones [4, 5] for various lignins.

The more expanded DHPGS monolayer has higher values for the ΔV potential (Table 1) owing to the fact that more polar groups interact with the molecules from the subphase. The presence of methoxyl groups in DHPGS molecules increases the mean monomer dipole moment, which is higher than for the others lignins. At alkaline pH, the ΔV potential values are higher compared with the other two polymers. On one hand, this is due to the first term in Eq. (4), but on the other hand, it is a consequence of the smaller screening effect by the counterions. From Table 1 it is seen that the number of charges per monomer area is the smallest. This is very likely a result of the presence of more β-0–4 links. These bonds are formed with the participation of phenolic groups, so the interfacial density of potential ion-forming groups is decreased.

Monolayer stability and rheological properties

Compressed lignin monolayers are far from equilibrium. Slow surface pressure relaxations have been observed after stopping the monolayer compression or in surface pressure–area hysteresis [4, 5]. These effects are related to the molecular reorganization of the lignin molecules at the air–water interface, although partial dissolution into the aqueous subphase cannot be completely excluded.

A usual test of monolayer stability consists in compressing the monolayer after spreading to a given value of the surface pressure and then recording the relative decrease in area $\frac{\Delta A}{A}$ with time t at constant surface pressure. The experimental curves $\frac{\Delta A}{A}(t)$ depend strongly on the quantity spread and on the rate and magnitude of the consecutive compression. As an example in Fig. 7 $\frac{\Delta A}{A}(t)$ curves are presented for D-L spread layers (3 mgm^{-2} at pH 1.2) with a surface pressure of about 2 $mNm^{-1}$and consecutive compression to 2.5 (curve 1), to 3.5 mNm^{-1} (curve 2) and to 5 mNm^{-1} (curve 3). It should be noted that the surface pressure after spreading is not an equilibrium one; on the other hand the $\frac{\Delta A}{A}(t)$ dependences are obtained after large compressions. Far from equilibrium the kinetic effects are nonlinear and the quantitative interpretation of the observed effects is a difficult task.

In order to compare the instability of D-L, DHPG and DHPGS monolayers the following procedure was adopted: spreading of 2 mgm^{-2} (a quasi-monolayer organization of the 3D lignin molecules) and 6 mgm^{-2} (lignin molecules involved in a 3D network) and a consecutive compression leading to a 1–1.5 mNm^{-1} surface pressure increase. The results obtained are presented in Fig. 8. The slopes $\frac{1}{A(t)}\frac{d(\Delta A)}{dt}$give the relative rate of the reorganization process. The values of $\frac{1}{A(t)}\frac{d(\Delta A)}{dt}$ are maximal at the beginning of the process and decrease with time. After about 1 h a steady state with a minimal rate is reached. The values of the initial and minimal reorganization rates are calculated from Fig. 8 and are presented in Table 2 together with the values of the relative decrease of area at 1 h. The observed rates and the relative decrease of the area depend on the interfacial

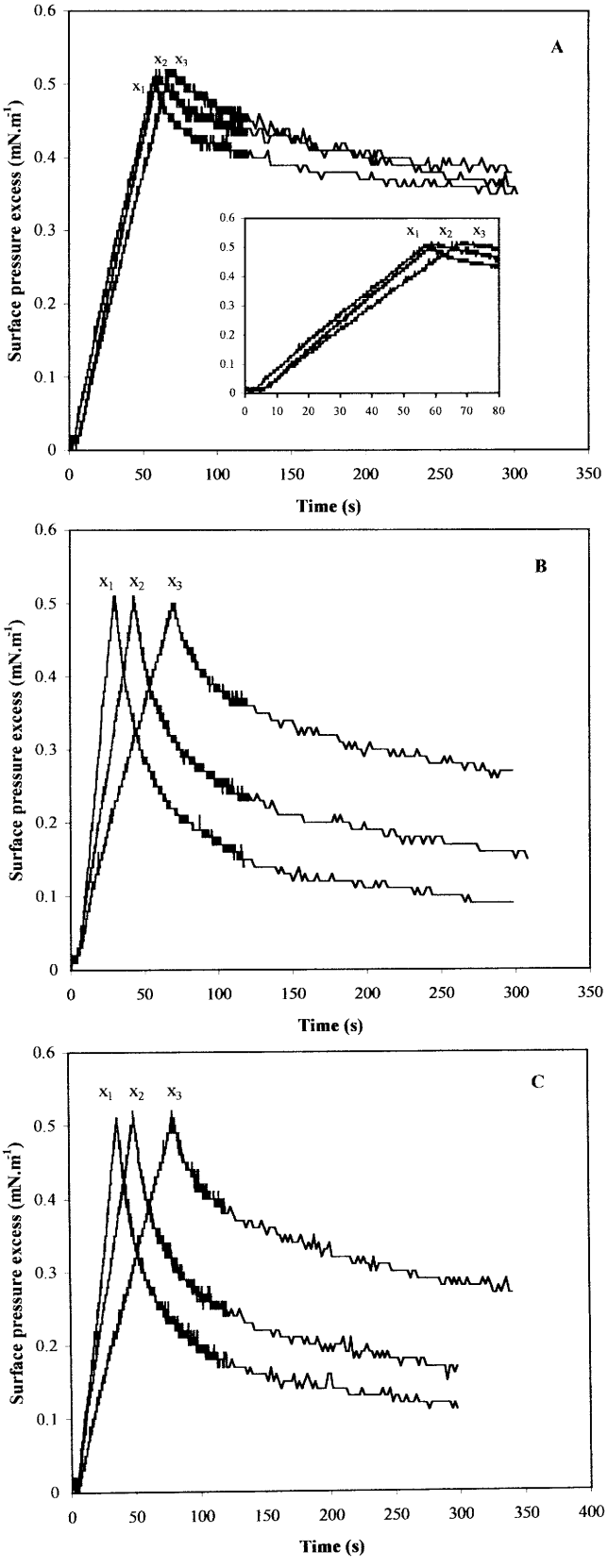

Fig. 12a–c. Surface pressure change, $\Delta\pi$, with time, t, at various distances, x, during a compression with $U_b = 10$ cm^{2}min^{-1} and the consecutive relaxation of lignin monolayers with a spread amount of 6 mgm^{-2} on a subphase with pH 5.8. **a** D-L, $x_1 = 8$ cm, $x_2 = 20$ cm, $x_3 = 36$ cm; **b** DHPG, $x_1 = 6$ cm, $x_2 = 17$ cm, $x_3 = 29$; **c** DHPGS, $x_1 = 8$ cm, $x_2 = 20$ cm, $x_3 = 31$ cm

organization of the films, the chemical structure of the polymers and the pH. The films with a quasi-monolayer organization of the 3D lignin molecules, obtained after spreading 2 mgm^{-2} are more stable than the films organized as a 3D network in the case of deposited 6 mgm^{-2}. For the latter, the stability of the lignin films decreases in the order D-L, DHPG and DHPGS. The D-L monolayer on the subphase with pH 11 seems more stable than at the acidic pH. The reason could be related to the presence of linked phenolic acids.

From the data in Table 2 it should be concluded that slow reorganization processes with characteristic times of several thousands of seconds and more occur.

In order to get other information on the structural reorganization of the layers in the quasi-steady-state regime with the minimal rate, electrical and optical measurements were performed (Fig. 9). It is clear from the surface potential evolution measured in barostatic conditions with a spread amount of 1 mgm^{-2} that the ΔV potential is practically constant during the whole experiment and that it slightly decreases with a spread amount of 6 mgm^{-2}.

Similarly the absolute value of the ellipticity in Brewster-angle conditions measured at constant area after a compression is practically constant with a spread amount of 1 mgm^{-2} and slightly decreases with a spread amount of 6 mgm^{-2}. In the two cases a relative thermodynamic nonequilibrium situation is noted from the evolution of the area or of the pressure. From the ellipticity data it can be concluded that the number of the molecules per unit area remains constant in the 2D system or decreases slightly in the 3D system during the reorganization processes.

As already discussed, the quantitative interpretation of $\frac{\Delta A}{A}(t)$ kinetic curves is a difficult task. The dynamic response of the lignin surface film for the characteristic times in the range of one to several hundred seconds can be quantitatively analyzed during and after small well-defined changes in the surface pressure. Typical results for $\Delta\pi(x, t)$ obtained during and after compressions with two different rates, $U_b = 10$ and 180 cm^{2}min^{-1}, for lignin films formed after spreading on an aqueous subphase (pH 5.8) of 2 mgm^{-2} are presented in Figs. 10 and Fig. 11, respectively. Elastic behavior during the compression is observed because the slopes $\left(\frac{d(\Delta\pi)}{dt}\right)_x$ in the quasi-steady region do not depend on the distance x, according to Eq. (18). The relaxation process is observed

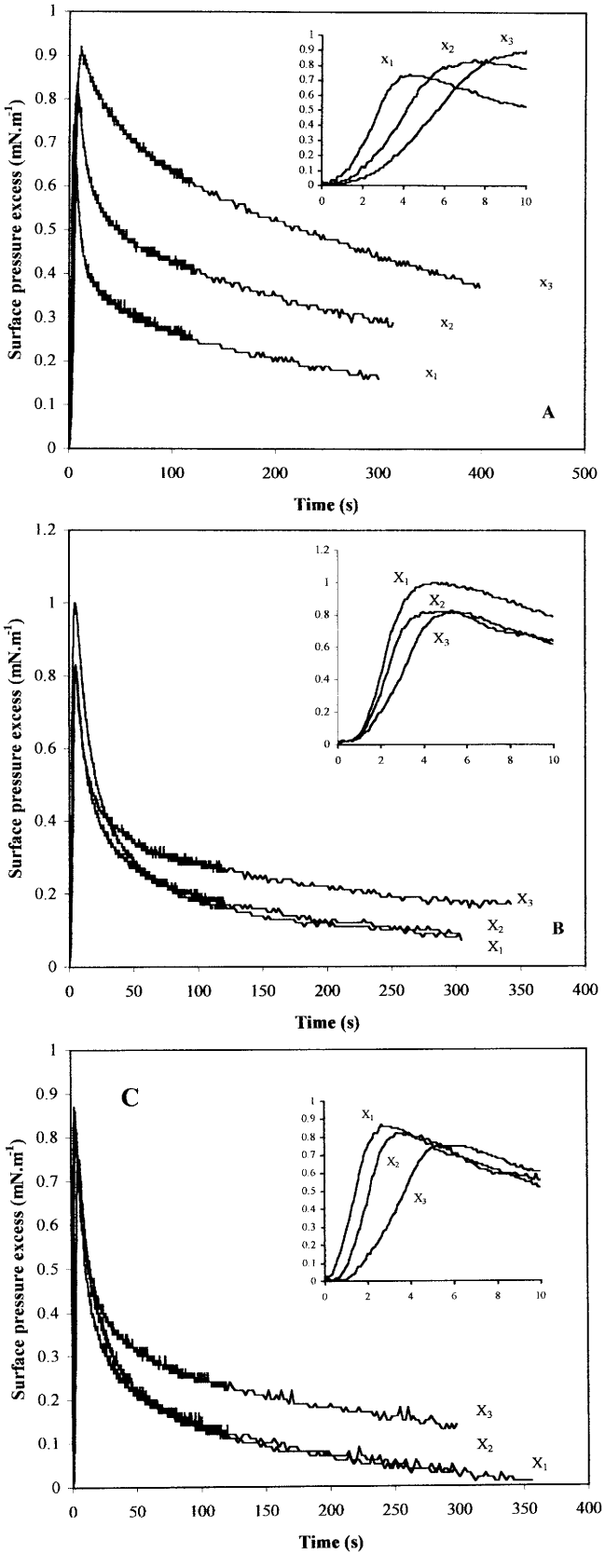

Fig. 13a–c. Surface pressure change, $\Delta\pi$, with time, t, at various distances, x, during a compression with $U_b = 180$ cm^{2}min^{-1} and the consecutive relaxation of lignin monolayers with a spread amount of 6 mgm^{-2} on a subphase with pH 5.8. **a** D-L, $x_1 = 8$ cm, $x_2 = 20$ cm, $x_3 = 36$ cm; **b** DHPG, $x_1 = 6$ cm, $x_2 = 17$ cm, $x_3 = 29$; **c** DHPGS, $x_1 = 8$ cm, $x_2 = 20$ cm, $x_3 = 31$ cm

after stopping the compression and can be analyzed for $T \ll \tau_1$, τ_2 by means of Eq. (21) and the data in Fig. 11. The data obtained for E_e, E_{ne}, τ_1 and τ_2 for all the pH studied are presented in Table 3.

The typical results for $\Delta\pi(x, t)$ obtained for lignin films formed after spreading 6 mgm^{-2} are presented in Figs. 12 and Fig. 13. Viscoelastic behavior (a fanlike dependence) during the compression is observed. The relaxation process, which occurred after stopping the compression, is analyzed for $T \ll \tau_1$, τ_2 by means of Eq. (21) and the data in Fig. 13. Thus, the values of τ_1 and τ_2 are obtained and they are presented in Table 3. The characteristic time, θ, responsible for the observed viscoelastic behavior during the compression and the values for E_e and E_{ne} were calculated using Eq. (24) and they are presented in Table 3. The calculation was performed by using the values for τ_1 for the rapid compression ($T \approx \tau_1$) and with those of τ_2 for slow compression ($T \approx \tau_2$).

From the data in Table 3 it should be concluded that during the compression the lignin monolayers, organized in a quasi-monolayer structure (2 mgm^{-2}), behave as an elastic 2D body. In this structure two reorganization processes occur with characteristic times of about 10 and 100 s. In contrast, the 3D network of lignin molecules (6 mgm^{-2}) has viscoelastic behavior with three reorganization times of about 1, 10 and 100 s.

The part of the nonequilibrium elasticity, accumulated during the compression and dissipated through an unknown molecular mechanism $\frac{E_{ne}}{E_e+E_{ne}}100\%$, is also presented in Table 3. The more pronounced stability of D-L in comparison with the films of model polymers DHPG is consistent with the data from Table 2. For the two model lignins, speculation concerning the interfacial organization can be made on the basis of Tables 2 and Table 3. Using these data, the comparison between the synthetic lignins shows that for a spread amount of 2 mgm^{-2} at acidic pH (1.2 and 5.8), DHPGS forms more stable (slow reorganization rate) and less dense monolayers (low values for the elasticity) than DHPG. In contrast, for a spread quantity of 6 mgm^{-2} the 3D network stability is similar for both polymers.

These assumptions are partially supported by the observations made in Ref. [12] that at low spread quantities the DHPs behave completely differently, while at high spread amounts, the structure differences of the layers are smoothed.

Acknowledgements Our warm thanks to B. Monties for his interest and fruitful discussion in the course of this work. The help provided by Anela Ivanova for the molecular model is greatly appreciated. The program Cocop from the Ministère des Affaires Etrangères DSUR-NGE-4C1-6 financially supported this work.

Appendix

Numerical calculation of E_{ne}. From the fit procedure based on Eq. (21) in the form

$$\pi(t) = \pi_e + A_1 \exp(-t/\tau_1) + A_2 \exp(-t/\tau_2) \qquad (A1)$$

where

$$A_1 = (\pi_0 - \pi_\infty)\frac{E_{ne_1}}{E_{ne_1} + E_{ne_2}}$$

and

$$A_2 = (\pi_0 - \pi_\infty)\frac{E_{ne_2}}{E_{ne_1} + E_{ne_2}}$$

and the experimental data obtained from the relaxation after the compression with $U_b = 180$ cm^{2}min^{-1}, the values for τ_i are obtained. From the compression performed with $U_b = 10$ cm^{2}min^{-1} we take the value of $\Delta\pi_e$ because at the end of the experiment the relaxation processes are finished ($T > \theta$, τ_1, τ_2).

Then, for the case with 2 mgm^{-2} we use Eq. (13) and (18) to find E_{ne} in such a manner that the calculated value for $d\Delta\pi/dt$ to be equal to the experimental slope from the compressions (i.e. we use E_{ne} as a fit parameter).

For a spread quantity of 6 mgm^{-2}, we calculate E_{ne} using Eqs. (24) and (25) and different values for α. Finally, we choose that value for α for which the least-squares standard deviation is minimal. Using the relationship $\alpha^{-1} = \sqrt{D_u\theta}$, we find the characteristic time θ presented in Table 3.

References

1. Adler E (1997) Wood Sci Technol 11:169
2. Nimz H (1974) Angew Chem Int Ed Engl 13:313
3. Karhunen P, Sipilä J, Rummahko P, Brunow G (1995) Tethrahedron Lett 36:169
4. Luner P, Kempf U (1970) TAPPI 53:2069–2076
5. Barros AM, Dhanabalan A, Constantino CJL, Balogh DT, Oliveira ON Jr (1999) Thin Solid Films 354:215–221
6. Luner P, Roseman G (1986) Holzforschung 40:61–66
7. Cathala B, Puff N, Aguié-Béghin V, Douillard R, Monties B (2000) In: Glasser WG, Northey RA, Schultz TP (eds) Lignin: historical, biological, and materials perspective. ACS symposium series 742. American Chemical Society, Washington, DC, pp 278–290
8. Constantino CJL, Juliani PL, Botaro VR, Balogh DT, Pereira MR, Ticianelli EA, Curvelo AAS, Oliveira ON Jr (1996) Thin Solid Films 284–285:191–194
9. Constantino CJL, Dhanabalan A, Curvelo AAS, Oliveira ON Jr (1998) Thin Solid Films 327–329:47–51
10. Baumberger S, Aguié-Béghin V, Douillard R, Lapierre C, Monties B (1997) Ind Crops Products 6:259–263
11. Gilardi G, Cass AEG (1993) Langmuir 9:1721–1726
12. Cathala B, Lee LT, Aguié-Béghin V, Douillard R, Monties B (2000) Langmuir 16:10444
13. Manning-Benson S, Bain CD, Darton RC (1997) J Colloid Interface Sci 189:109
14. Davis JT, Rideal EK (1961) Interfacial phenomena. Academic, New York, p 72
15. Earnshaw JC (1993) In: Feast WJ, Munro HS, Richards RW (eds) Polymer surfaces and interfaces II. Wiley, Chichester, p 101
16. Langevin D, Bouchiat AM (1971) CR Acad Sci Paris Ser B 272:1422
17. Hard S, Jofgren H (1977) J Colloid Interface Sci 60:529
18. Lucassen-Reynders EH (1983) In: Lucassen-Reynders EH (ed) Anionic surfactant. Dekker, New York, p 173
19. Lucassen-Reynders EH, Lucassen J (1969) Adv Colloid Interface Sci 2:347
20. Mann JA (1972) In: Good RJ, Stroberg RR, Patrick RL (eds) Techniques of surface chemistry and physics, vol 1. Dekker, New York, p 77
21. Lucassen J, Barnes GT (1972) J Chem Soc Faraday Trans I 68:2129
22. Edwards D, Brenner H, Wasan DT (1991) In: Interfacial transport processes and rheology. Butterworth-Heinemann, Woburn, Mass
23. Van Voorst Vader F, Erkens JF, Van den Temple M (1964) Trans Faraday Soc 60:1170
24. Panaiotov I (2000) Ann Univ Sofia Fac Chim 88:121
25. Dimitrov D, Panaiotov I (1975/76) Ann Univ Sofia Fac Chim 70:103
26. Dimitrov D, Panaiotov I, Richmond P, Ter-Minassian Saraga L (1978) J Colloid Interface Sci 65:483
27. Panaiotov I, Dimitrov DS, Ter-Minassian Saraga L (1979) J Colloid Interface Sci 72:49
28. Panaiotov I, Dimitrov DS, Ivanova M (1979) J Colloid Interface Sci 69:318
29. Panaiotov I, Sanfeld A, Bois A, Baret JFJ (1983) Colloid Interface Sci 96:315
30. Bois A, Panaiotov I (1995) J Colloid Interface Sci 170:25
31. Loglio G, Tesei U, Miller R (1991) Colloids Surf 61:219
32. Boury F, Ivanova T, Panaiotov I, Proust JE, Bois A, Richou J (1995) J Colloid Interface Sci 169:380
33. Dimitrov DS, Panaiotov I (1980) In: Georgiev G (ed) Prog. II symposium "Lung lipid metabolism...", Varna, 19–24 May 1979. Publishing House of the Bulgarian Academy of Sciences, Sofia, p 19
34. Grozev N, Minkov I, Panaiotov I (2001) Ann Univ Sofia, Fac Chim (submitted)
35. Adamson AW (1976) Physical chemistry of surfaces. Wiley, New York, p 110
36. Hall PL, Glasser WG, Drew SW (1981) In: Kirk K (ed) Lignin biodegradation: microbiology, chemistry and applications. CRC, Boca Raton, pp 33–49
37. Shigematsu HSM, Shinoda Y, Tanashi M (1995) Mokuzai Gakkaishi 41:1151